Equilibrium and Transition between Single- and Double-Headed Binding of Kinesin as Revealed by Single-Molecule Mechanics

Kenji Kawaguchi,* Sotaro Uemura,* and Shin'ichi Ishiwata*†
*Department of Physics, School of Science and Engineering, †Advanced Research Institute for Science and Engineering, and Materials Research Laboratory for Bioscience and Photonics, Waseda University, 3-4-1 Okubo, Shinjuku-ku, Tokyo 169-8555, Japan

ABSTRACT Kinesin is a processive motor protein that "walks" on a microtubule toward its plus end. We reported previously that the distribution of unbinding force and elastic modulus for a single kinesin-microtubule complex was either unimodal or bimodal depending on the nucleotide states of the kinesin heads, hence showing that the kinesin may bind the microtubule either with one head or with both heads at once. Here, we found that the shape of the unbinding-force distribution depends both on the loading rate and on the manner of loading not only in the presence of AMP-PNP but also in the absence of nucleotides. Irrespective of the nucleotide state and the loading conditions examined here, the unbinding force obtained by loading directed toward the minus end of microtubule was 45% greater than that for plus end-directed loading. These results could be explained by a model in which equilibrium exists between single- and double-headed binding and the load (F) dependence of lifetime, $\tau(F)$, of each binding is expressed by $\tau(F) = \tau(0)\exp(-Fd/k_BT)$, where $\tau(0)$ is the lifetime without external load and d a characteristic distance, both of which depend on single- or double-headed binding, k_B, the Boltzmann constant and T, the absolute temperature. The model analysis showed that the forward and backward rates of transition from single- to double-headed binding are 2 and 0.2/s for the AMP-PNP state, and 70 and 7/s for the nucleotide-free state. Moreover, in the presence of AMP-PNP, we detected the moment of transition from single- to double-headed binding through an abrupt increase in the elastic modulus and estimated the transition rate to be ~1/s, which is consistent with the model analysis.

INTRODUCTION

Kinesin is a processive molecular motor that transports vesicles and organelles toward the plus end of a microtubule, i.e., from the central region to the periphery of various cells (Vale, 1999; Hirokawa, 1998). Upon binding to a microtubule, kinesin takes more than 100 consecutive steps before dissociating, with each step measuring 8 nm, a distance equal to the size of a single heterodimer subunit of the microtubule (Block et al., 1990; Svoboda et al., 1993; Howard, 1996; Vale et al., 1996). Each step taken is coupled to one cycle of ATP hydrolysis (Hua et al., 1997; Schnitzer and Block, 1997; Mandelkow and Johnson, 1998; Coy et al., 1999). The run length, a measure of processivity, estimated in a single molecular in vitro assay, is ~1 μm and depends on such experimental variables as ionic strength (Block et al., 1990; Vale et al., 1996) and temperature (Kawaguchi and Ishiwata, 2000; 2001b). Kinesin's high processivity has been explained by a model in which the two heads of kinesin alternate repeatedly between single-headed and double-headed binding to a microtubule, which allows for movement accompanied by ATP hydrolysis (Hackney, 1994; Cross, 1995; Rice et al., 1999; Vale and Milligan, 2000).

To investigate the binding mode of kinesin with microtubules at various nucleotide states, we measured the mechanical properties of a single kinesin-microtubule complex (Kawaguchi and Ishiwata, 2001a), including the unbinding force and the elastic modulus, by using optical tweezers (Nishizaka et al., 1995). Conventional two-headed kinesin molecules purified from bovine brain were attached to a polystyrene bead in a 1:1 molar ratio, and each bead was manipulated with optical tweezers on a microtubule that was adsorbed on to a coverslip (Svoboda and Block, 1994; Higuchi et al., 1997; Kojima et al., 1997). An external load was imposed on the attached kinesin molecule either by moving the bead toward the plus or minus end of the microtubule, or alternatively, moving the microscope stage on which the microtubule was mounted.

In the previous paper (Kawaguchi and Ishiwata, 2001a), we found that kinesin is involved primarily in single-headed binding in the absence of nucleotides (nucleotide-free state; strictly speaking, the absence of exogenous nucleotides) and in the coexistence of ADP and AMP-PNP, and double-headed binding in the presence of AMP-PNP (AMP-PNP state), which is consistent with the current model of kinesin motility. Here, we found that the average unbinding force and the apparent ratio between single- and double-headed binding in the unbinding-force distribution were dependent on the loading direction and the loading rate, respectively. Additionally, we could detect the moment of transition from single- to double-headed binding in the AMP-PNP state through an abrupt increase in the elastic modulus during loading, and estimated that the transition rate from the single- to double-headed binding was ~1/s. We have shown that all the data could be explained by a model in which equilibrium exists between single- and double-headed binding (the transition rate between the two binding states is assumed) and detachment from the microtubule occurs during either single- or double-headed binding. We conclude that the

Submitted July 15, 2002, and accepted for publication October 23, 2002.
Address reprint requests to Dr. Shin'ichi Ishiwata, Department of Physics, School of Science and Engineering, Waseda University, 3-4-1 Okubo, Shinjuku-ku, Tokyo 169-8555, Japan. Tel.: +81-3-5286-3437; Fax: +81-3-5286-3437; E-mail: ishiwata@waseda.jp.

0006-3495/03/02/1103/11 $2.00

double-headed binding state is predominant under equilibrium in the absence of external load not only in the AMP-PNP state, but also in the nucleotide-free state.

Double-headed binding was not detected in the nucleotide-free state in the previous study (Kawaguchi and Ishiwata, 2001a) due to the fact that the loading rate used was significantly lower than the rate constant for the transition between single- and double-headed binding in the nucleotide-free state, which was an order-of-magnitude larger than that in the AMP-PNP state. In general, the lower the loading rate, the higher the probability of unbinding at single-headed binding.

MATERIALS AND METHODS

Proteins

Kinesin and tubulin were prepared from bovine (Kojima et al., 1997) and porcine (Hyman, 1991) brains, respectively. Polarity-marked microtubules labeled with tetramethylrhodamine succinimidyl ester (Molecular Probes, Eugene, OR) were prepared according to Hyman (1991) except that the tubulin used was not N-ethylmaleimide(NEM)-treated, hence polymerization also occurred at the minus end (compare to Fig. 2 *A* in Kawaguchi and Ishiwata, 2001a).

Bead assay

Kinesin-coated beads were prepared according to the established procedure (Kojima et al., 1997) except that yellow-green fluorescent latex beads were used (1.0 μm in diameter, carboxylate-modified; Molecular Probes). Kinesin molecules were mixed with the beads at a molar ratio of 1:1. The average number of functional kinesin molecules per bead was estimated to be 1 by statistical methods (Svoboda and Block, 1994). Polarity-marked fluorescent microtubules in an assay buffer (2 mM $MgCl_2$, 80 mM PIPES-KOH, pH 6.8, and 1 mM EGTA) were introduced into a flow cell and incubated for 2 min to allow for binding to the glass surface. The solvent was exchanged with an assay buffer containing 0.7 mg/ml filtered casein to coat the glass surface with casein. The flow cell was then filled with an assay buffer containing the kinesin-coated beads, filtered casein, and an enzymatic oxygen-scavenging system, and sealed with enamel (nail polish). The final solvent condition was ~0.1 pM kinesin-coated beads, 2 mM $MgCl_2$, 80 mM PIPES-KOH, pH 6.8, 1 mM EGTA, 0.7 mg/ml filtered casein, 1 U/ml apyrase (nucleotide-free state), or 1 mM AMP-PNP (AMP-PNP state), 10 μM taxol, 10 mM dithiothreitol (DTT), 4.5 mg/ml glucose, 0.22 mg/ml glucose oxidase, and 0.036 mg/ml catalase. As nucleotide-free kinesin is reportedly unstable in the absence of microtubule (Crevel et al., 1996), apyrase (a scavenger of ATP and ADP) was added just before each measurement. We were able to measure the unbinding force repeatedly on the same bead, and confirmed that there was no significant difference in either the unbinding force distribution or binding properties regardless of the presence or absence of apyrase. It is therefore unlikely that kinesin denatured during measurement in the absence of nucleotides. However, it should be noted that we found that kinesin eventually failed to attach to the microtubules after ~30 min from the addition of apyrase, suggesting that kinesin was denatured due to prolonged incubation with apyrase. Hence the data acquisition was always completed within ~10 min after the addition of apyrase. We confirmed that kinesin molecules moved toward the plus end of the polarity-marked microtubules in the presence of ATP. When the external load was imposed, either the trap center or the glass cover (only at the highest loading rate in Fig. 2 *b*) was moved at a constant rate. The proportion of beads that underwent the binding-unbinding cycle was ~40% of the total examined, whereas the proportion in which unbinding did not occur even at the largest external load imposed by optical tweezers (~20 pN) was less than 5%. The remaining beads (~60%) failed to bind even after three trials of steps *1–2* in Fig. 1. All experiments were performed at 25 ± 1°C.

Apparatus

The microscopy system employed was equipped with optical tweezers as previously described (Nishizaka et al., 1995; 2000) and already applied for studies of the mechanics of the kinesin-microtubule interaction (Kawaguchi and Ishiwata, 2000; 2001a). Stiffness of the optical trap was estimated to be 0.087 pN/nm based on two kinds of techniques as previously described (Nishizaka et al., 1995).

Model analysis

For the model analysis, in which equilibrium is assumed to exist between attached and detached states, and also between single- and double-headed binding states of kinesin, we calculated the time dependence of the proportion of attached kinesin molecules, $N(t)$, using *Mathematica* for *Windows*.

RESULTS

Measuring the unbinding force of a kinesin-microtubule complex

As shown schematically in Fig. 1, the bead in the medium was first trapped by optical tweezers, *1*, and placed in contact with a microtubule for 20–30 s (from *1* to *2*), which is considered sufficient time for realizing the binding equilibrium between kinesin molecule and a microtubule in the absence of loading, *2*. The trap center was then moved at a constant rate toward either the plus or minus end of the microtubule (from *2* to *3*). After the bead was moved following the trap center for some distance, regardless of the loading rates and solvent conditions, the load began to be imposed on the kinesin-microtubule complex from the point

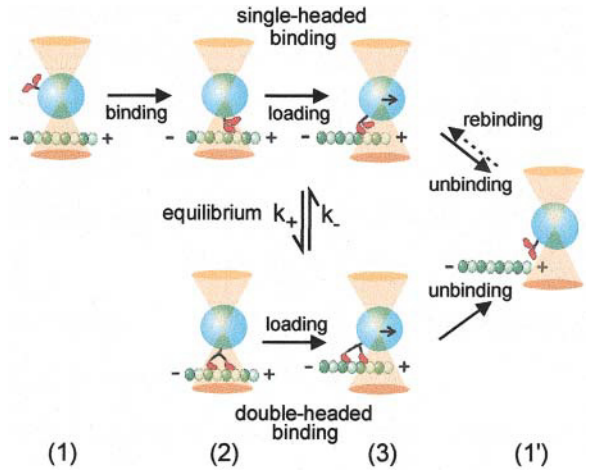

FIGURE 1 Schematic illustration showing the binding states of kinesin with a microtubule and measurement procedures. We assume that equilibrium exists between single- and double-headed binding with the rate constants k_+ and k_- (for more details, see text).

where the bead started to deviate from the trap center (*3*; loading direction shown by small arrows at the bead).

Upon imposition of the external load, unbinding between kinesin and the microtubule occurred from *3* to *1′* (termed ''initial unbinding''). This cycle (from *1* to *1′*) could be repeated several times for the same bead on the same microtubule. When the trap center was kept moving along the microtubule after the initial unbinding (from *3* to *1′*), rebinding (from *1′* to *3*) and subsequent unbinding (from *3* to *1′*) sometimes occurred (termed ''subsequent unbinding''). As reported previously (Kawaguchi and Ishiwata, 2001a), we were able to repeat the unbinding force measurements on the same microtubule several times for the same bead, presumably for the same kinesin molecule.

With a single molecule forming the attachment between the bead and the microtubule, it is possible for the bead to move some distance relative to the microtubule without deviating from the trap center, mainly because of rotational movement of the bead within the trap. This rotational movement does not register on the position detector. As observed in Figs. 2 *a* and 3 *a*, for the first part of the movement of the bead, the kinesin may be attached to the microtubule but this does not show in the displacement until the bead-kinesin-microtubule link tautens. Based on the size and geometry of the kinesin-tethered bead (Svoboda and Block, 1994; radius of bead, 0.5 μm; length of kinesin, 60 nm), the largest displacement required before the external load is imposed for the initial unbinding event is ~600 nm. In fact, this average displacement was as large as 300 nm (compare with Kawaguchi and Ishiwata, 2001a). Thus, unbinding data for beads that were displaced further than 600 nm before imposition of the external load began for the initial unbinding event were regarded as subsequent unbinding data but not initial unbinding data (~10% of measured beads for the AMP-PNP state; not observed for the nucleotide-free state).

Unbinding force distribution in the nucleotide-free state

Unbinding force measurements were performed at various loading rates (Figs. 2 and 3). Here, note that the loading rate was determined from the difference between the velocity of the moving bead and the average rate of extension of the protein-bead complex, so that it differed for every experiment. First, in the nucleotide-free state, unbinding occurred once (Fig. 2 *a*), but the subsequent rebinding and unbinding process (between *1′* and *3* in Fig. 1) could not be observed when the bead was kept moving along the microtubule at a velocity of between 20 and 130 nm/s, even after moving for several seconds. Inasmuch as the unbinding force measurements could be repeated several times for the same beads (Kawaguchi and Ishiwata, 2001a), this was probably not due to the denaturation of kinesin but rather to a small (re)binding rate constant in the nucleotide-free condition. A

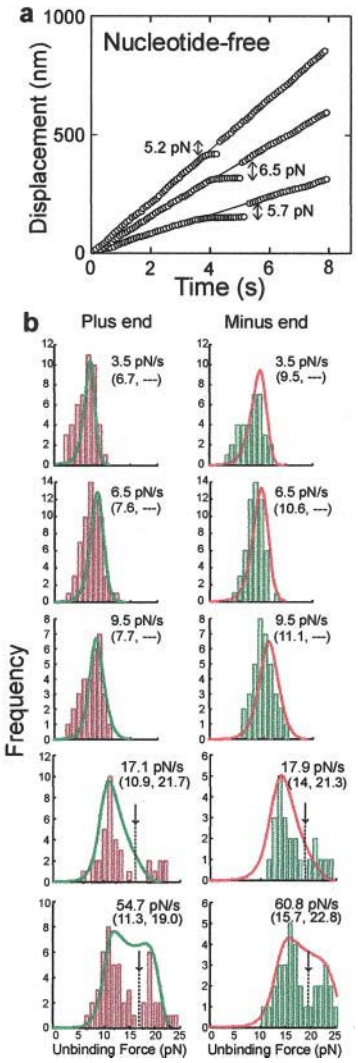

FIGURE 2 Loading rate dependence of unbinding force distribution in the nucleotide-free state. Unbinding force was measured by loading toward either the plus end (*a* and *left column* in *b*) or the minus end (*right column* in *b*). (*a*), Examples showing the time course of movement of the trap center (*thin lines*) and a bead (*circles*) at various moving velocities (110, 75, and 40 nm/s from *top* to *bottom*). (*b*), Histograms showing unbinding force distribution at various loading rates (*pN/s*) for the plus end (*pink*) or minus end (*light green*) loading. At the loading rate higher than 50 pN/s, the glass cover was moved instead of the trap center, so that the position of the trap center was fixed. Note that the loading rate was determined either simply from the moving velocity of the bead (only at the highest loading rate) or from the difference between the moving velocity of the bead and the average extension velocity (see the *insert* of Fig. 4 *a*) of the kinesin-microtubule-bead complex, so that the loading rate was different at every measurement even if the moving velocity of the bead is the same. (*Dotted lines with arrow*), The boundary between *S*- and *L*-components, were determined by eye. Average unbinding force (*pN*) for the *S*- and *L*-components is shown in parentheses. On simulation curves for unbinding-force distribution (*green curves* for the plus-end loading, and *red curves* for the minus-end loading), see the model analysis in Discussion and Fig. 6.

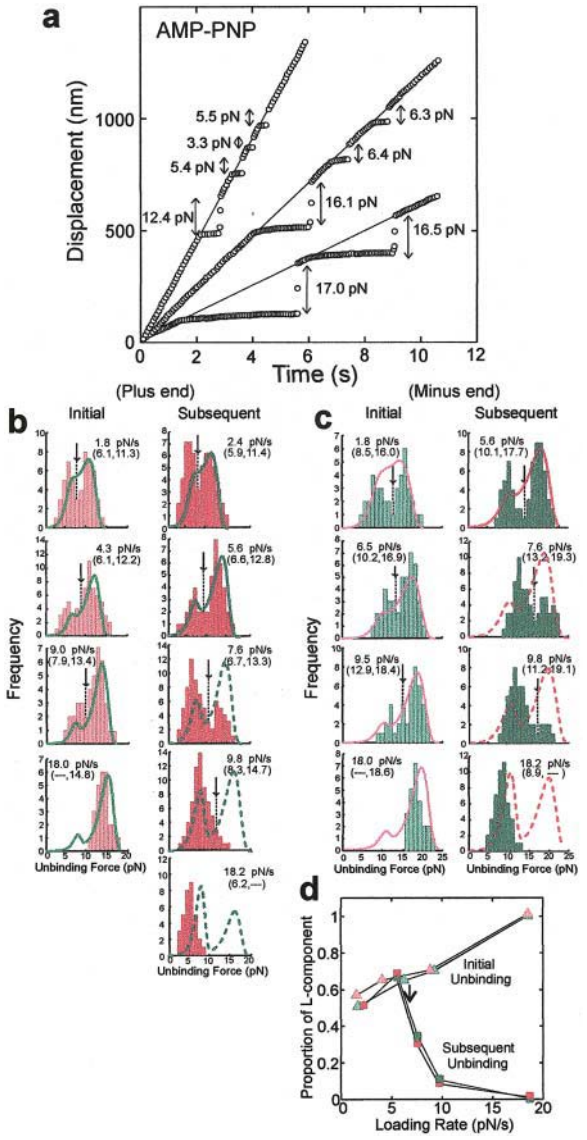

FIGURE 3 Loading-rate dependence of unbinding force distribution in the AMP-PNP state. Unbinding force was measured by loading toward either the plus end (*a* and *b*) or the minus end (*c*). (*a*), Examples showing the time course of movement of the trap center (*thin lines*) and bead (*circles*) at various moving velocities (110, 75, and 40 nm/s from *top* to *bottom*). (*b*) and (*c*), Histograms showing unbinding-force distribution at various loading rates (*pN/s*; see the legend of Fig. 2) for the plus end (*red*) or minus end (*green*) loading, and for the initial unbinding (*left columns* in *b* and *c*, shown by *light red* and *light green*, respectively) and subsequent unbinding (*right columns* in *b* and *c*, shown by *dark red* and *dark green*, respectively). Dotted lines with arrow, the boundary between *S*- and *L*-components, were determined by eye. Average unbinding force (*pN*) for the *S*- and *L*-components is shown in parentheses. On simulation curves for unbinding-force distribution (*green curves* for the plus-end loading and *red curves* for the minus-end loading), see the model analysis in Discussion and Fig. 6. The *dashed curves* show the results of simulation that deviated significantly from the data. (*d*), Loading-rate dependence of the proportion of *L*-component for the initial unbinding (*triangles*) and subsequent unbinding (*squares*). Data shown by *light* and *dark red* (or *light* and *dark green*) symbols were obtained from the *left* and *right columns* of *b* (or from the *left* and *right* columns of *c*), respectively. *Arrow*, see Discussion.

series of histograms showing the dependence on loading rate of the unbinding force distribution in the nucleotide-free state is summarized in Fig. 2 *b*. When the loading rate was increased from 3.5 to 9.5 pN/s, where the unbinding-force distribution was unimodal, the average unbinding force increased by 15% from 6.7 to 7.7 pN for the plus-end loading, and from 9.5 to 11.1 pN for the minus-end loading. With a further increase in the loading rate from ~17 to 60 pN/s, the unbinding force distribution tended to become bimodal, with the second peak corresponding to an unbinding force about twice as large as that at which the first peak appears. We call the former the small unbinding force (*S*-) component and the latter the large unbinding force (*L*-) component. It should be noted that, irrespective of the type of distribution, i.e., either unimodal or bimodal, the average unbinding force for minus-end loading was larger by 45% than that for plus-end loading at each loading rate. We tried to simulate the unbinding force distribution based on a model, for which results are shown by solid curves in Fig. 2 *b* (For details, see Discussion).

Unbinding force distribution in the AMP-PNP state

In the presence of AMP-PNP, the rebinding-unbinding cycle recurred once or a few times subsequent to the initial unbinding, during which the bead was kept moving (even as fast as 200 nm/s) along the microtubule (Fig. 3 *a*). The frequency of subsequent unbinding events was several times per μm of microtubule. Rebinding of kinesin to the microtubule was estimated to take an average of 2–3 s after unbinding in the subsequent unbinding events, which suggests that rotation of the bead may have occurred after unbinding, as is also the case in the initial unbinding events.

The left-most columns of Fig. 3, *b* and *c* show the dependence of the unbinding force distribution on loading rate for the initial unbinding event for the plus-end and minus-end loading, respectively. The unbinding force distribution was bimodal. A remarkable feature is that the proportion of the *S*-component decreased proportionally with the loading rate. At the highest loading rate examined (18.0 pN/s), the *S*-component disappeared, leaving only the *L*-component. This phenomenon is the same as that in the nucleotide-free state, although the loading rate at which the transition from the *S*-component to the *L*-component occurred was lower in the AMP-PNP state than in the nucleotide-free state. Also, as is the case with the nucleotide-free state (Fig. 2 *b*), when the loading rate was increased, the average unbinding force increased for both the *S*- and *L*-components regardless of loading direction. Furthermore, the average unbinding forces of the *S*- and *L*-components measured for minus-end loading were larger by ~45% than those for plus-end loading at all loading rates.

In contrast to that for the initial unbinding, the unbinding force distribution for subsequent unbinding showed a rather

different tendency (right-most columns of Fig. 3, *b* and *c*). As the loading rate was increased, the proportion of the *L*-component increased once, and then eventually disappeared. This characteristic is clearly seen in Fig. 3 *d*: at the highest loading rate, the initial unbinding contained only the *L*-component, whereas subsequent unbinding contained only the *S*-component. At loading rates less than ~6 pN/s, however, the unbinding-force distributions obtained under the two different procedures became indistinguishable. It should also be noted that in the subsequent unbinding (irrespective of the loading direction), the average unbinding force of *S*-component, which increased by 10–40% on increasing the loading rate from 2.4 to 9.8 pN/s, decreased by 20–30% when the loading rate was increased still further, from 9.8 to 18.2 pN/s. These characteristics have been explained by a model as described below in the Discussion. The simulation curves are overlaid in Fig. 3, *b* and *c*, with those that deviated significantly from (qualitatively different from) the data indicated by dashed curves (for more details, see Discussion).

Elastic modulus of a kinesin-microtubule complex

We estimated the elastic modulus of kinesin molecules and examined its relation to the unbinding force. Fig. 4 *a* shows an example of the force-extension relation for plus-end loading in the nucleotide-free state. Unlike that for complexes of F-actin and heavy meromyosin (Fig. 2 *b* of Nishizaka et al., 1995), ~40% of data showed a linear relationship as shown in Fig. 4 *a*, and the remaining 60% of data were scattered to some extent, but all the data could be simulated by a straight line by the least squares fit. Thus, the elastic modulus could be estimated from the slope of the line to be 0.35 ± 0.14 ($n = 46$), 0.34 ± 0.18 ($n = 62$), and 0.40 ± 0.18 ($n = 31$) pN/nm, respectively, at 3.5, 6.5, and 9.5 pN/s, which appears to be independent of loading rate (Fig. 4 *b*). The elastic modulus obtained for minus-end loading was 0.38 ± 0.15 ($n = 34$), 0.41 ± 0.17 ($n = 56$), and 0.37 ± 0.19 ($n = 36$) pN/nm, respectively, at 3.5, 6.5, and 9.5 pN/s. Thus, the elastic modulus was independent not only of the loading rates within the range we examined but also the loading direction.

In contrast to the nucleotide-free state, the force-extension relation in the AMP-PNP state showed a complex characteristic. The force-extension relation depended on whether the unbinding event was the initial or the subsequent one. That is, the relation for the initial unbinding was always linear irrespective of the *S*-component (data not shown) or the *L*-component (see Fig. 5 *a*), and the elastic modulus of the *S*-component was nearly equal to that in the nucleotide-free state (see Fig. 4 *a*). That is, the elastic modulus of the *S*- and the *L*-component was, respectively, 0.36 ± 0.15 ($n = 23$) and 0.77 ± 0.29 ($n = 30$) pN/nm for the plus-end loading, and 0.33 ± 0.18 ($n = 19$) and 0.81 ± 0.21 ($n = 21$) pN/nm for the minus-end loading at the loading rate of 1.8 pN/s. Just as in the nucleotide-free state, the elastic modulus was independent of the loading rate examined and the loading direction.

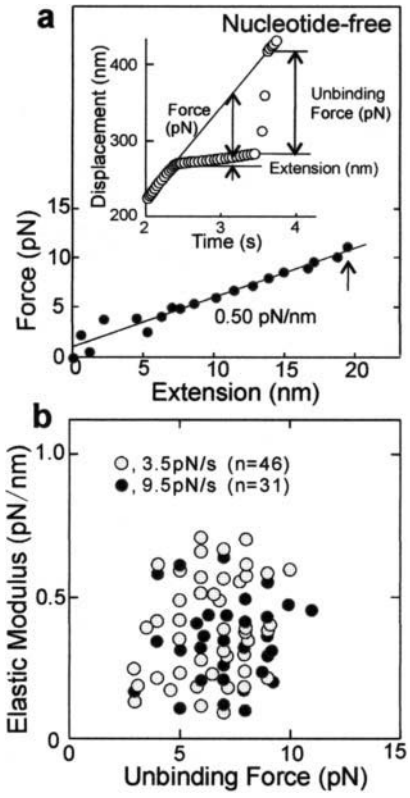

FIGURE 4 Relation between the elastic modulus and unbinding force for the *S*-component of kinesin molecules measured by the plus-end loading in the nucleotide-free state. (*a*), The force-extension relation was obtained from the time course of bead displacement (*insert*; Kawaguchi and Ishiwata, 2001a; Nishizaka et al., 1995) at the loading rate of ~9 pN/s (see the legend of Fig. 2). Strictly speaking, the force means the force component parallel to the glass surface, and the extension means the displacement of the bead in parallel to the glass surface (see Discussion). An arrow shows the moment at which unbinding occurred. The elastic modulus was estimated from the slope of the thin line (this datum is included in *b*). (*b*), Relation between the elastic modulus and unbinding force at different loading rates, 3.5 pN/s (*gray circles*) and 9.5 pN/s (*black circles*), shown in the left column of Fig. 2 *b*. The elastic modulus (Mean ± SD, unit in pN/nm) is 0.35 ± 0.14 ($n = 46$) for 3.5 pN/s and 0.40 ± 0.18 ($n = 31$) for 9.5 pN/s.

On the other hand, the force-extension relation for the subsequent unbinding was linear (composed of single phase) for all the data for the *S*-component (not shown). The elastic modulus obtained from this relation was 0.39 ± 0.17 ($n = 14$) pN/nm for the plus-end loading and 0.42 ± 0.11 ($n = 25$) pN/nm for the minus-end loading at a loading rate of 5.6 pN/s. As for the *L*-component, ~25% of the force-extension relation was broken once in the middle (composed of double phase as shown in Fig. 5 *a*) and half of the remaining 75% appeared to be linear, whereas the other was not clearly identified as the data points were somewhat scattered. They could, however, be simulated by a straight line. The elastic

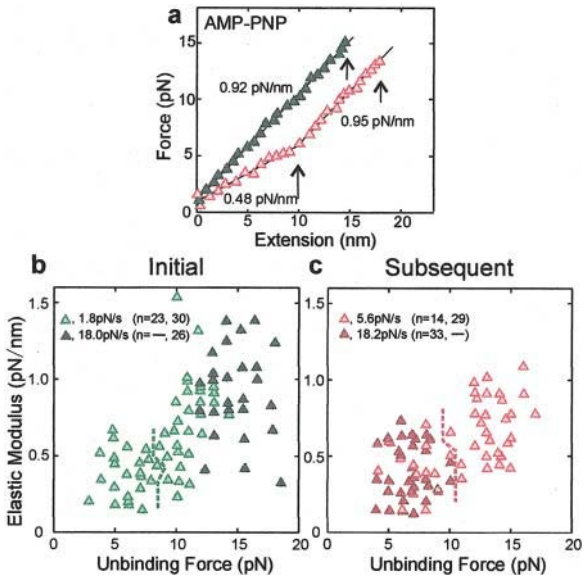

FIGURE 5 Relation between the elastic modulus and unbinding force of kinesin molecules measured by the plus-end loading in the AMP-PNP state. (*a*), Examples showing the force-extension relation obtained from the time course of bead displacement (see Fig. 4 *a*) for the initial unbinding (*dark green*) and the subsequent unbinding (*pink*). Short arrows show the moment at which the detachment of kinesin occurred. A long arrow shows the moment at which the transition occurred from a smaller to a larger slope. Data shown by dark green and pink were included in one of the data shown in *b* and *c*, respectively. (*b*) and (*c*), Relation between the elastic modulus and unbinding force for the initial unbinding measurements (*b*, compare with *left column* of Fig. 3 *b*) at 1.8 pN/s (*light green*) and 18.0 pN/s (*dark green*), and for the subsequent unbinding measurements (*c*, compare with *right column* of Fig. 3 *b*) at 5.6 pN/s (*pink*) and 18.2 pN/s (*red*). When the force-extension relation was once broken at the middle, both initial and final slopes were plotted in *c*. The two regions separated by a dashed line correspond to the *S*- and *L*-components determined in Fig. 3 *b*. The elastic modulus (Mean ± SD, unit in pN/nm; *S*- and *L*-components, respectively) is (0.36 ± 0.15 ($n = 23$), 0.77 ± 0.29 ($n = 30$)) at 1.8 pN/s and (−, 0.86 ± 0.28 ($n = 26$)) at 18.0 pN/s for the initial unbinding, and (0.39 ± 0.17 ($n = 14$), 0.67 ± 0.21 ($n = 29$)) at 5.6 pN/s and (0.38 ± 0.19 ($n = 33$), −) at 18.2 pN/s for the subsequent unbinding.

modulus obtained from the data categorized to the latter type, either linear or scattered, was 0.71 ± 0.15 ($n = 8$) and 0.65 ± 0.12 ($n = 11$) pN/nm for the plus-end loading and 0.68 ± 0.15 ($n = 9$) and 0.62 ± 0.18 ($n = 25$) pN/nm for the minus-end loading at the loading rate of 5.6 pN/s.

As for data showing the double phase, the second slope (0.95 pN/nm in the example shown in Fig. 5 *a*) coincided with the slope of the *L*-component (0.92 pN/nm in the example shown in Fig. 5 *a*) in the initial unbinding (see Fig. 5 *b*). The first slope of the double phase (0.48 pN/nm in the example shown in Fig. 5 *a*) coincided with the slope of the *S*-component (Fig. 5, *b* and *c*). The average values of the elastic modulus for the first and the second slope of the double phase were 0.33 ± 0.14 and 0.69 ± 0.10 ($n = 10$) pN/nm, respectively, for plus-end loading and 0.31 ± 0.12 and 0.64 ± 0.15 ($n = 6$) pN/nm for minus-end loading at a loading rate of 5.6 pN/s. Again, the elastic modulus appears to be independent of the loading rate we examined and the loading direction (data not shown).

Finally, we determined the time at which the transition occurred from the first slope to the second slope in the force-extension relation that showed a double-phase in the subsequent unbinding. Although the shape of distribution could not be determined due to the lack of data ($n = 30$), the transition time was distributed from zero to 1.6 s and the average time was determined to be ~1 s, irrespective of the loading rate and the loading direction: that is, 1.11 ± 0.23 s ($n = 20$) for plus-end loading and 1.18 ± 0.17 s ($n = 10$) for minus-end loading.

DISCUSSION

Single- and double-headed binding of kinesin

The findings that the unbinding force and elastic modulus were classified into two groups with values differing by a factor of nearly 2 are attributable to single- (Figs. 2 *b* and 4 *b*) and double-headed binding (Fig. 3, *b* and *c*, Fig. 5, *b* and *c*; and Kawaguchi and Ishiwata, 2001a). Direct evidence for this explanation was recently obtained by using a one-headed construct of kinesin heterodimer. The unbinding-force distribution was unimodal and the average unbinding force coincided with that of *S*-component for the conventional two-headed kinesin homodimer used here (Uemura et al., 2002).

The above situation is analogous to that examined using AFM that showed the unbinding force for a pair of streptavidin-biotin complexes to be twice as large as that for a single complex (Wong et al., 1998). Our finding that the average unbinding force increased with increasing a loading rate (Fig. 2 *b* and Fig. 3, *b* and *c*) is consistent with AFM measurement for streptavidin-biotin complexes (Merkel et al., 1999), suggesting that this property is common to protein-protein interactions. This property has also been explained by the present model analysis.

Binding mode of kinesin in the AMP-PNP state and in the nucleotide-free state

As can be seen from Fig. 3, the fact that the *L*-component was predominant at 18 pN/s, the highest loading rate for the initial unbinding (the *bottom* of the *left column* in Fig. 3, *b* and *c*), implies that double-headed binding is predominant at equilibrium in the absence of external load in the AMP-PNP state. If the loading rate used to cause unbinding is significantly larger than the rate constants of the single-to-double-headed binding equilibrium, the unbinding-force distribution is expected to reflect the distribution at the binding equilibrium. This interpretation has been confirmed by the model analysis described below (Fig. 6).

Furthermore, in the nucleotide-free state, the *L*-component appeared to increase with the loading rate (Fig. 2 *b*). It

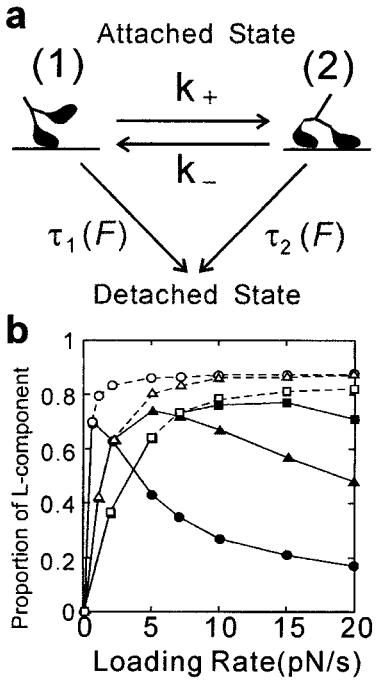

FIGURE 6 Scheme to explain the dependence on loading rate and loading direction of the average unbinding force and the unbinding-force distribution. (*a*), A model where equilibrium is assumed to exist between single-headed (*1*) and double-headed (*2*) binding with the rate constants, k_+ and k_-, between the two binding states. The lifetime, the inverse of the detachment rate, of each binding state is expressed as $\tau_i(F) = \tau_i(0)\exp(-F \times d_i/k_BT)$ (i = 1, 2), where d_i is a characteristic distance, k_B Boltzmann constant and T the absolute temperature (compare with Nishizaka et al., 2000). In this model calculation, the value of $\tau(0)$ was determined according to experimentally derived values (Hancock and Howard, 1999), so that the adjustable parameters were d, k_+ , and k_-. (*b*), According to the above model, we tried to determine the most appropriate values of rate constants to reproduce the data shown in Fig. 3 *d*, i.e., the loading-rate dependence of the proportion of the *L*-component for the initial and subsequent unbinding in the presence of AMP-PNP. Here, we show the results of model simulation for plus-end loading in the AMP-PNP state where the kinetic constants, k_+ and k_-, were changed keeping the equilibrium constant, i.e., the ratio k_+/k_-, as 10 considering that the values of $\tau_1(0)$ and $\tau_2(0)$ were, respectively, chosen as 150 and 2000 s, so that the ratio of $\tau_1(0)$ and $\tau_2(0)$ was ~1:10. *Open* and *solid symbols*, respectively, show the initial and the subsequent unbinding, in which we assumed that the values of k_+ and k_- did not depend on the initial or the subsequent unbinding. The values of k_+ and k_- (1/s) chosen were, respectively, 0.5 and 0.05 (*circles*); 2 and 0.2 (*triangles*); and 5 and 0.5 (*squares*).

should, however, be noted that the transition of the unbinding-force distribution from the *S*-component to the *L*-component occurred at a much higher loading rate (above 50 pN/s), than the few pN/s in the AMP-PNP state. The model described below has also explained these properties (Fig. 6).

It can be inferred that the *S*-component was, on the other hand, predominant at the highest loading rate, for the subsequent unbinding in the AMP-PNP state (the *bottom* of the *right column* in Fig. 3, *b* and *c*) is due to the unbinding of the attached head during single-headed binding before the attachment of the second head of the kinesin molecule, inasmuch as the loading rate was too high for the transition from single- to double-headed binding to occur. This inference could also be confirmed according to the same model as described below. It must be stressed that the only difference between the initial and the subsequent unbinding in the model analysis was in the initial conditions. The proportion of single- and double-headed bindings was 1:10 for the former and 1:0 for the latter, implying that the results obtained by two different methods could be explained by the same mechanism.

In the AMP-PNP state, at loading rates lower than ~5.6 pN/s, corresponding to a rate constant of 0.8 /s (= (5.6 pN/s)/(7 pN)), the proportion of double-headed binding for the initial and subsequent unbinding coincided as shown in Fig. 3 *d*. This is probably because, at such low loading rates, the binding equilibrium is attained throughout loading, thus the unbinding-force distribution becomes independent of the initial conditions. Fig. 3 also shows that the proportion of double-headed binding decreased markedly on further lowering of the loading rate, which is reasonable as the probability of unbinding during single-headed binding is higher at a lower loading rate.

The data summarized in Fig. 3 *d* are expected to contain information on the rate constants, k_+ and k_-, for transition between single- and double-headed bindings (compare to Fig. 1). As for the subsequent unbinding in the AMP-PNP state, k_+ can be estimated as 1/s (= (7.0 pN/s)/(7 pN)) by assuming that the unattached second head binds during the period in which the first head is still attached, and considering that the average unbinding force for single-headed binding is 7 pN and the proportion of double-headed binding becomes 50% at the loading rate 7.0 pN/s (see *arrow* in Fig. 3 *d*). This consideration had been more directly detected as a change in the elastic modulus during loading (Fig. 5 *a*). The time over which the transition occurred was estimated as ~1 s, which is consistent with the above estimation for k_+.

It is intriguing that the loading-rate dependence of unbinding force distribution, determined primarily by k_+ in our scheme, was independent of loading direction. This property seems to be in contrast with that of the active state in the presence of ATP, where kinesin's walking velocity is increased by the plus-end loading (Coppin et al., 1997) or the loading perpendicular to the microtubule (Gittes et al., 1996), so that k_+ is expected to depend on the loading direction. Thus, the above property may be intrinsic to the equilibrium state attained in the absence of nucleotides and in the presence of AMP-PNP.

It should be noted that the average unbinding force dropped significantly at the highest loading rate during subsequent unbinding (*right-most columns* in Fig. 3, *b* and *c*). The scheme described below could not explain this result (see the large deviation, especially on the peak position, from that of the distribution obtained by the model analysis). This may be explained by taking into account the presence of two binding sites, weak and strong, within each head (Woehlke

et al., 1997; Hirose et al., 1995; Crevel et al., 1996; Uemura et al., 2002), meaning that in the subsequent unbinding, the weak single-headed binding may occur first, so that at the highest loading rate, the single-headed binding may detach before the attached head undergoes the transition from weak to strong binding. This proposal does not contradict the fact that the elastic modulus remained unchanged despite the decrease in the average unbinding force (Fig. 5 *c*) because the most compliant part may not exist near the binding site. This should be confirmed experimentally in the future by using one-headed kinesin instead of conventional two-headed kinesin (Uemura et al., 2002).

Model analysis

We have done a model analysis as shown in Fig. 6 to explain the above results, particularly *1*) the loading-rate dependence of the average unbinding force and the unbinding force distribution, not only in the absence of nucleotides (Fig. 2 *b*) but also for both the initial and the subsequent unbinding in the presence of AMP-PNP (Fig. 3, *b* and *c*), and *2*) the dependence on the loading direction of unbinding force obtained under all the conditions examined.

First, we analyzed the dependence on time (t) and external load (F) of the proportion of the attached state of kinesin, $N(t, F)$, according to the scheme illustrated in Fig. 6 *a*. In the case of the one-headed kinesin heterodimer previously examined (Uemura et al., 2002), the unbinding is assumed to occur through a single step (only *state 1* is present in Fig. 6 *a*). In the present study, $N(t, F)$ is a function of only t because F is expressed as $F = \alpha t$, where α is a constant loading rate. Thus, $N(t)$ is expressed as $N(t) = N(0)\exp(-t/\tau(F))$, where $N(0)$ is the proportion of the attached state at time zero and $\tau(F)$ is a binding lifetime dependent on F, such that τ is also a function of only t in the present study. Here, we assume that, according to the results for an actin-myosin (HMM and S1) rigor complex (Nishizaka et al., 2000), $\tau(F) = \tau(0)\exp(-Fd/k_BT) = \tau(0)\exp(-\alpha d/k_BT)t = \tau(t)$, where $\tau(0)$ is a lifetime in the absence of external load, 150 s (Hancock and Howard, 1999; Uemura et al., 2002), d a characteristic distance, k_B the Boltzmann constant and T the absolute temperature. This model could simulate not only the increase in the average unbinding force with increasing loading rate but also predicts the unbinding force to be greater by 45% for minus-end loading compared with plus-end loading by assuming the d value for the plus-end loading (d_+) as 4.0 nm and that for minus-end loading (d_-) as 3.0 nm (compare with Uemura et al., 2002).

Conversely, when conventional two-headed kinesin homodimer was used, the results were not so simple. To explain the present results (Figs. 3 and 5; see also Fig. 2 in Kawaguchi and Ishiwata, 2001a), we assume that equilibrium exists between single- and double-headed binding as illustrated in Fig. 6 *a*. We also assume that the detachment of kinesin from a microtubule occurs during both single- and double-headed binding with different $\tau(0)$ values and characteristic distances (in contrast to the model by Strunz et al., 2000). Thus, $N_1(t)$ and $N_2(t)$, respectively the proportion of single-headed and double-headed binding, obey the following differential equations:

$$\frac{dN_1(t)}{dt} = k_- N_2(t) - \left\{k_+ + \frac{1}{\tau_1(t)}\right\} N_1(t) \qquad (1)$$

$$\frac{dN_2(t)}{dt} = k_+ N_1(t) - \left\{k_- + \frac{1}{\tau_2(t)}\right\} N_2(t) \qquad (2)$$

where the relation $N_1 + N_2 = 1$ is always maintained. After the above differential equations (Eqs. 1 and 2) are solved, the unbinding force distribution, $P(F(t))$, can be obtained by the following derivative (Eq. 3):

$$P(F(t)) = \frac{d(N_1(t) + N_2(t))}{dt} = \frac{N_1(t)}{\tau_1(t)} + \frac{N_2(t)}{\tau_2(t)} \qquad (3)$$

Here, the histogram of the unbinding force distribution can be obtained by $P(t)dt$ (or $P(F)dF$), i.e., the probability for the unbinding to occur between t and $t + dt$ (or between F and $F + dF$).

We assume the direct detachment from double-headed binding because the unbinding force distribution becomes very broad without this assumption (compare with Strunz et al., 2000). It is inferred that the load imposed on the attached head is instantaneously doubled upon detachment of one of two attached heads, so that for a kinesin molecule engaged in double-headed binding to a microtubule, the detachment of the remaining attached head occurs immediately after one head detaches, which is equivalent to the *simultaneous* detachment of both heads from the microtubule. In practice, we have never observed a moment at which a single-headed binding appeared to occur immediately after the double-headed unbinding occurred (see a record of the time course of the bead displacement shown in Figs. 2 *a*, 3 *a*, and 4 *a*). To detect the transient state of single-headed binding, higher time resolution may be needed.

In the model analysis, to reproduce the loading-direction and the loading-rate dependence of the unbinding force, the values of $\tau_1(0)$ and $\tau_2(0)$ were chosen as 150 s and 2000 s, respectively, and the values of d_1 and d_2 were 4.0 and 3.0 nm, respectively, for the plus-end loading (+), and 3.0 and 2.5 nm, respectively, for the minus-end loading (−; see Table 1; compare with Uemura et al., 2002). The lifetime of double-headed binding state, $\tau_2(0)$, shown in the model (*state 2* in Fig. 6 *a*) was determined to be 2000 s so as to make the *average* lifetime of the two-headed kinesin-microtubule complex equal to the 1000 s experimentally determined in the absence of external load (Hancock and Howard, 1999), where $\tau_1(0)$ was fixed as 150 s. The average lifetime, 1000 s, did not depend on the absolute values of k_+ and k_- as far as the ratio of k_+ and k_- was kept constant, 10. As the ratio of $\tau_1(0)$ and $\tau_2(0)$ was chosen as ~1:10, $N_1(0)$

TABLE 1 Parameters used for model analysis

		AMP-PNP		Nucleotide-free	
		initial	subsequent	initial	
$\tau_1(0)$, $\tau_2(0)$	[s]	150, 2000	150, 2000	150, 2000	
$d_{+(1)}$, $d_{+(2)}$	[nm]	4.0, 3.0	4.0, 3.0	4.0, 3.0	
$d_{-(1)}$, $d_{-(2)}$		3.0, 2.5	3.0, 2.5	3.0, 2.5	
$N_1(0)$, $N_2(0)$		1/11, 10/11	1, 0	1/11, 10/11	
k_+, k_-	[1/s]		2.0, 0.2	2.0, 0.2	70, 7

and $N_2(0)$ were, respectively, chosen as 1/11 and 10/11 (i.e., $k_+/k_- = 10$) for the initial unbinding event. Here, the initial unbinding is assumed to occur after the binding equilibrium is attained. On the other hand, $N_1(0)$ and $N_2(0)$ for the subsequent unbinding event were chosen as 1 and 0, respectively, because it is assumed that the subsequent unbinding event always starts from single-headed binding. As a result of computer analysis (an example is shown in Fig. 6 *b*), the values of k_+ and k_- were chosen as 2.0 and 0.2/s, respectively, for the AMP-PNP state and 70 and 7/s, respectively, for the nucleotide-free state for the best fit of simulation (keeping the ratio 10).

Thus, the above model analysis was able to simulate the essential features of the unbinding force distribution (see *solid curves* in Fig. 2 *b*, and Fig. 3, *b* and *c*) when a set of parameters indicated with triangles in Fig. 6 *b* was chosen. However, this simple model could not simulate the abrupt decrease in N_2 at higher than 5 pN/s for the subsequent unbinding (compare Fig. 6 *b* with Fig. 3 *d*, and also see *dashed curves* in Fig. 3, *b* and *c*). This large deviation observed in the subsequent unbinding at higher loading rates could be improved upon by considering the large dependence of k_+ and/or k_- on the loading rate. For example, as shown in Fig. 6 *b*, if the rate constants, 2 and 0.2/s at 5 pN/s is lowered to 0.5 and 0.05/s at 7.5 pN/s, the large loading-rate dependence observed in Fig. 3 *d* can be simulated. The loading-rate dependence of the rate constants may suggest that the visco-elastic properties of kinesin-microtubule complex could play a role in the forced unbinding.

We did not need to take into account the load (and loading-rate) dependence of the rate constants, k_+ and k_- for the initial unbinding. However, this does not necessarily mean that the rate constants are insensitive to external load during the initial unbinding but that the introduction of load-dependent rate constants did not improve the simulation as far as the present model is concerned. Also, note that the unbinding-force distribution in the nucleotide-free state was obtained only for the initial unbinding, in which the shape of distribution was almost independent of whether or not the load dependence of the rate constants was taken into account or not.

Thus, the time and load dependence of the number (or the proportion when normalized) of the kinesin-microtubule binding for the initial and the subsequent unbinding have been simulated. The parameters finally determined as the best to simulate the data are summarized in Table 1. The unbinding force distribution thus obtained reproduced the characteristics of experimental results (as shown by *solid curves* in Fig. 2 *b* for the nucleotide-free state and Fig. 3, *b–d* for the AMP-PNP state). It should be stressed that the initial and subsequent unbinding in the model analysis differed solely in the initial conditions (see the legend of Fig. 6); it was not necessary to change the values of other parameters.

The major difference observed in the initial unbinding between the nucleotide-free state and the AMP-PNP state was that the loading rate at which the transition between unimodal and bimodal distributions occurs was larger for the nucleotide-free state (larger than 50 pN/s, see Fig. 2 *b*) than for the AMP-PNP state (smaller than 2 pN/s, see Fig. 3, *b–d*). In the present model, this difference was attributable to the difference in the rate constants between single- and double-headed binding: that is, the model predicts that the rate constants for the former, 70 and 7/s, are an order-of-magnitude larger than those for the latter, 2 and 0.2/s (Table 1).

Asymmetry of mechanical properties, loading direction, and its physiological implication

A simple explanation for the dependence of the unbinding force on loading direction (Figs. 2 and 3) is that the load imposed toward the minus end is effectively smaller than that toward the plus end. This is conceivable if the part of neck linker of kinesin, through which the external load is imposed, is connected to the head part facing to the minus end of kinesin, being asymmetric against the binding interface (Rice et al., 1999). This will cause the asymmetrical geometry of the point of action of external load. Hence, the external load is imposed on the kinesin-microtubule binding interface asymmetrically (see the illustration of kinesin molecule in Fig. 1; see Rice et al., 1999, and Hoenger et al., 2000).

In our model analysis, the asymmetry of the unbinding force was attributed to the difference in the characteristic distance, d, which is larger for plus-end loading than for minus-end loading. This implies that the effective load required to induce the unbinding is smaller for plus-end loading, which is consistent with the above interpretation.

The smaller unbinding force for plus-end loading seems to indicate that it is favorable for kinesin to walk toward the plus end of a microtubule. Upon double-headed binding, the two heads are bridged. If the leading head pulls the trailing head and vice versa, the binding of the trailing head will thus become unstable compared with that of the leading head even if both heads are in the same nucleotide state (compare with Uemura et al., 2002). Moreover, if this destabilization of the binding of the trailing head due to forward pulling is coupled to the attachment or detachment of nucleotides, that is, if such a synchronization occurs within a molecule through mechano-chemical coupling, directional movement

of kinesin molecules on microtubule will be possible through the repetition of alternating single- and double-headed binding.

Relation between lifetime and unbinding force for kinesin-microtubule complex

The lifetime of kinesin-microtubule complex, which is related to the binding energy, has been measured in the absence of external load to be ~1000 s in both the nucleotide-free and AMP-PNP states for two-headed kinesin and ~100 s for one-headed kinesin (Hancock and Howard, 1999). The present experiments showed that the average lifetime of the attached state decreased to ~1 s at 10 pN. Assuming that the relation between the binding lifetime (τ) and the external load (F) is expressed as $\tau(F) = \tau(0)\exp(-Fd/k_BT)$ as in the case of the rigor bond of acto-heavy meromyosin complexes (Nishizaka et al., 1995; 2000), the present model analysis showed that the d value most appropriate for simulating the data was 3.0–4.0 nm for the plus-end loading and 2.5–3.0 nm for the minus-end loading. Our preliminary experiments on the load dependence of the binding lifetime in the presence of AMP-PNP supported this estimate (Seo and Ishiwata, unpublished results). This value is an order-of-magnitude larger than that for the average protein-protein interaction (compare with Nishizaka et al., 2000). Thus, we propose that such a large characteristic distance may be inherent to motor proteins.

Extension of a kinesin-microtubule complex

The extension of kinesin molecules, at which unbinding occurred, can be estimated from the ratio of the unbinding force and the elastic modulus as ~18 nm for the plus-end loading (or 21 nm for the minus-end loading) regardless of conditions. However, this estimate is only an apparent one. Taking into account the fact that the radius of bead is 0.5 μm and that the length of kinesin is 60 $\pm$ 20 nm (Svoboda and Block, 1994), the extension of kinesin corresponding to the 18 (or 21) nm displacement of bead is estimated to be 8.3 $\pm$ 1 (9.7 $\pm$ 1) nm, which is ~18 (or 21) nm $\times$ cos(θ), where θ (1.1 $\pm$ 0.1 rad) is the angle between the long axis of kinesin and the glass surface (Kawaguchi and Ishiwata, 2001a). However, the extension of 8.3 (or 9.7) nm may still be too large for the small protein molecules such as kinesin. Such a large extension may be attributable not only to the extension and partial unfolding, e.g., forced unzippering of neck linker region (Rice et al., 1999) of each head of kinesin, but also to that of the binding region of the tubulin heterodimer.

In conclusion, the present study has demonstrated that single molecule measurements of the unbinding force and the elastic modulus can determine the manner and kinetics of kinesin binding to a microtubule under various nucleotide-binding states.

We thank Dr. K. Kinosita, Jr. of Okazaki National Research Institute and Dr. T. Nishizaka of Kansai Advanced Research Center for continuous collaboration. We are grateful to Drs. Y. Y. Toyoshima and T. Yagi of The University of Tokyo for their suggestions on the preparation of kinesin and tubulin, and to Dr. H. Higuchi of Tohoku University for the kinesin bead assay protocol. We also thank Mr. Mark Chee of Duke University for his critical reading of the manuscript.

This research was partly supported by Grants-in-Aid for Specially Promoted Research, for Scientific Research on Priority Areas, and for the Bio-venture Project from the Ministry of Education, Sports, Culture, Science and Technology of Japan; and by the Mitsubishi Foundation.

REFERENCES

Block, S. M., L. S. B. Goldstein, and B. J. Schnapp. 1990. Bead movement by single kinesin molecules studied with optical tweezers. *Nature*. 348:348–352.

Coppin, C. M., D. W. Pierce, L. Hsu, and R. D. Vale. 1997. The load dependence of kinesin's mechanical cycle. *Proc. Natl. Acad. Sci. USA*. 94:8539–8544.

Coy, D. L., M. Wagenbach, and J. Howard. 1999. Kinesin takes one 8-nm step for each ATP that it hydrolyzes. *J. Biol. Chem*. 276:3667–3671.

Crevel, I. M., A. Lockhart, and R. A. Cross. 1996. Weak and strong states of kinesin and NCD. *J. Mol. Biol*. 257:66–76.

Cross, R. A. 1995. On the hand over hand footsteps of kinesin heads. *J. Muscle Res. Cell Motil*. 16:91–94.

Gittes, F., E. Meyhöfer, S. Baek, and J. Howard. 1996. Directional loading of the kinesin motor molecule as it buckles a microtubule. *Biophys. J*. 70:418–429.

Hackney, D. D. 1994. Evidence for alternating head catalysis by kinesin during microtubule-stimulated ATP hydrolysis. *Proc. Natl. Acad. Sci. USA*. 91:6865–6869.

Hancock, W. O., and J. Howard. 1999. Kinesin's processivity results from mechanical and chemical coordination between the ATP hydrolysis cycles of the two motor domains. *Proc. Natl. Acad. Sci. USA*. 96: 13147–13152.

Higuchi, H., E. Muto, Y. Inoue, and T. Yanagida. 1997. Kinetics of force generation by single kinesin molecules activated by laser photolysis of caged ATP. *Proc. Natl. Acad. Sci. USA*. 94:4395–4400.

Hirokawa, N. 1998. Kinesin and dynein superfamily proteins and mechanism of organelle transport. *Science*. 279:519–526.

Hirose, K., A. Lockhart, R. A. Cross, and L. A. Amos. 1995. Nucleotide-dependent angular change in kinesin motor domain bound to tubulin. *Nature*. 376:277–279.

Hoenger, A., M. Thormahlen, R. Diaz-Avalos, M. Doerhoefer, K. N. Goldie, J. Muller, and E. Mandelkow. 2000. A new look at the microtubule binding patterns of dimeric kinesins. *J. Mol. Biol*. 297: 1087–1103.

Howard, J. 1996. The movement of kinesin along microtubules. *Annu. Rev. Physiol*. 58:703–729.

Hua, W., E. C. Young, M. L. Fleming, and J. Gelles. 1997. Coupling of kinesin steps to ATP hydrolysis. *Nature*. 388:390–393.

Hyman, A. A. 1991. Preparation of marked microtubules for the assay of the polarity of microtubule-based motors by fluorescence. *J. Cell Sci*. 14:125–127.

Kawaguchi, K., and S. Ishiwata. 2000. Temperature dependence of force, velocity and processivity of single kinesin molecules. *Biochem. Biophys. Res. Commun*. 272:895–899.

Kawaguchi, K., and S. Ishiwata. 2001a. Nucleotide-dependent single- to double-headed binding of kinesin. *Science*. 291:667–669.

Kawaguchi, K., and S. Ishiwata. 2001b. Thermal activation of single kinesin molecules with temperature pulse microscopy. *Cell Motil. Cytoskeleton*. 49:41–47.

Kojima, H., E. Muto, H. Higuchi, and T. Yanagida. 1997. Mechanics of single kinesin molecules measurement by optical trapping nanometry. *Biophys. J.* 73:2012–2022.

Mandelkow, E., and K. A. Johnson. 1998. The structural and mechano-chemical cycle of kinesin. *TIBS.* 23:429–433.

Merkel, R., P. Nassoy, A. Leung, K. Ritchie, and E. Evans. 1999. Energy landscapes of receptor-ligand explored with dynamic force spectroscopy. *Nature.* 397:50–53.

Nishizaka, T., T. Miyata, H. Yoshikawa, S. Ishiwata, and K. Kinosita, Jr. 1995. Unbinding force of a single motor molecule of muscle measured using optical tweezers. *Nature.* 377:251–254.

Nishizaka, T., R. Seo, H. Tadakuma, K. Kinosita, Jr., and S. Ishiwata. 2000. Characterization of single actomyosin rigor bonds—load-dependence of lifetime and mechanical properties. *Biophys. J.* 79:962–974.

Rice, S., A. W. Lin, D. Safer, C. L. Hart, N. Naber, B. O. Carragher, S. M. Cain, E. Pechatnikova, E. M. Wilson-Kubalek, M. Whittaker, E. Pate, R. Cooke, E. W. Taylor, R. A. Milligan, and R. D. Vale. 1999. A structural change in the kinesin motor protein that drives motility. *Nature.* 402:778–784.

Schnitzer, M. J., and S. M. Block. 1997. Kinesin hydrolyses one ATP per 8-nm step. *Nature.* 388:386–390.

Strunz, T., K. Oroszlan, I. Schumakovitch, H.-J. Güntherodt, and M. Hegner. 2000. Model energy landscapes and the force-induced dissociation of ligand-receptor bonds. *Biophys. J.* 79:1206–1212.

Svoboda, K., C. F. Schmidt, B. J. Schnapp, and S. M. Block. 1993. Direct observation of kinesin stepping by optical trapping interferometry. *Nature.* 365:721–727.

Svoboda, K., and S. M. Block. 1994. Force and velocity measured for single kinesin molecules. *Cell.* 77:773–784.

Uemura, S., K. Kawaguchi, J. Yajima, M. Edamatsu, Y. Y. Toyoshima, and S. Ishiwata. 2002. Kinesin-microtubule binding is dependent on both nucleotide state and loading direction. *Proc. Natl. Acad. Sci. USA.* 99: 5977–5981.

Vale, R. D., T. Funatsu, D. W. Pierce, L. Romberg, Y. Harada, and T. Yanagida. 1996. Direct observation of single kinesin molecules moving along microtubules. *Nature.* 380:451–453.

Vale, R. D. 1999. Guidebook to the Cytoskeletal and Motor Proteins, 2nd ed. T. E. Kreis, editor. Oxford University Press, Oxford, England. 398–402.

Vale, R. D., and R. A. Milligan. 2000. The way things move: looking under the hood of molecular motor proteins. *Science.* 288: 88–95.

Woehlke, G., A. K. Ruby, C. L. Hart, B. Ly, N. Hom-Booher, and R. D. Vale. 1997. Microtubule interaction site of the kinesin motor. *Cell.* 90: 207–216.

Wong, S. S., E. Joselevich, A. T. Woolley, C. L. Cheung, and C. M. Lieber. 1998. Covalently functionalized nanotubes as nanometer-sized probes in chemistry and biology. *Nature.* 394:52–55.